Eddy current and coupled landscapes for nonadiabatic and nonequilibrium complex system dynamics

Kun Zhang[a], Masaki Sasai[b,c,d,1], and Jin Wang[a,e,1]

[a]State Key Laboratory of Electroanalytical Chemistry, Changchun Institute of Applied Chemistry, Chinese Academy of Sciences, Changchun, Jilin 130022, People's Republic of China; [b]Department of Computational Science and Engineering, Nagoya University, Nagoya 464-8603, Japan; [c]School of Computational Sciences, Korea Institute for Advanced Study, Seoul 130-012, Korea; [d]Okazaki Institute for Integrative Bioscience, Okazaki 444-8787, Japan; and [e]Department of Chemistry, Physics and Applied Mathematics, State University of New York at Stony Brook, Stony Brook, NY 11794

Edited by Peter G. Wolynes, Rice University, Houston, TX, and approved July 16, 2013 (received for review March 22, 2013)

Physical and biological systems are often involved with coupled processes of different time scales. In the system with electronic and atomic motions, for example, the interplay between the atomic motion along the same energy landscape and the electronic hopping between different landscapes is critical: the system behavior largely depends on whether the intralandscape motion is slower (adiabatic) or faster (nonadiabatic) than the interlandscape hopping. For general nonequilibrium dynamics where Hamiltonian or energy function is unknown a priori, the challenge is how to extend the concepts of the intra- and interlandscape dynamics. In this paper we establish a theoretical framework for describing global nonequilibrium and nonadiabatic complex system dynamics by transforming the coupled landscapes into a single landscape but with additional dimensions. On this single landscape, dynamics is driven by gradient of the potential landscape, which is closely related to the steady-state probability distribution of the enlarged dimensions, and the probability flux, which has a curl nature. Through an example of a self-regulating gene circuit, we show that the curl flux has dramatic effects on gene regulatory dynamics. The curl flux and landscape framework developed here are easy to visualize and can be used to guide further investigation of physical and biological nonequilibrium systems.

nonequilibrium landscape | adiabaticity | nonadiabaticity

Heterogeneity among coupled processes is a hallmark of complex behaviors of physical and biological systems. A photoexcited molecule, for example, may relax into different low-energy states depending on the difference among time scales of electronic and atomic motions. Molecular motors are fueled by ATP hydrolysis and move into the different structural states, where the heterogeneous distribution of time scales of reactions and structural changes should characterize the motor performance. Dynamical complexity owing to the interplay of heterogeneous processes with multiple time scales can give rise to rich phenomena.

In a system having multiple time scales, some dynamical quantities may take discrete values whereas others are continuous. An example of such heterogeneity is found in the electron-transfer reaction, in which the electronic state is discrete and atomic motions are continuous (1). Then, the system can be represented by multiple electronic energy surfaces and the change in atomic positions is motion along individual surfaces. Complex behaviors of the system are explained by the combined process of intrasurface motion along the same and intersurface hopping between different electronic energy surface(s). If the intrasurface motion is slower (faster) than the intersurface hopping, the process is called adiabatic (nonadiabatic). We here extend this notion, the significance of adiabatic and nonadiabatic effects, beyond the Hamiltonian systems to general nonequilibrium problems. Indeed, important complex systems such as reaction networks, gene switches, and molecular motors are constantly exchanging energy, materials, and information with their environments. For these pumped nonequilibrium systems, there is no Hamiltonian or energy surface given a priori, unlike the above example of the electron-transfer reaction.

For nonequilibrium systems, the concept of energy surface can be extended to the more general landscape picture: We previously showed that the driving force of stochastic motion in nonequilibrium systems is a sum of the gradient of the landscape and the curl flux on the landscape (2–7). Although the established framework is useful for addressing the global natures of complex systems (2–8), it has been applied only to a single landscape and is not directly applicable for multiple coupled landscapes. However, the adiabatic and nonadiabatic treatment of multiple energy surfaces taking into account the multiple time scales applies for the Hamiltonian systems where the energy function is a prior known for individual surfaces but does not directly apply to the case where the underlying process is nonequilibrium in nature.

Adiabatic and nonadiabatic nonequilibrium dynamics has been studied computationally or theoretically on gene switches (9–21) and molecular motors (22–24). However, a global description and framework of understanding is still challenging and in demand. Furthermore, although some systems have been studied computationally, the general complex systems require more intensive computations, and theoretical guidance is needed to develop an efficient algorithm for studying global dynamics. Finally, the ultimate goal is to uncover the underlying organization principle of the complex system and apply it to the design and engineering. Therefore, for general nonequilibrium complex dynamics where Hamiltonian or energy function is unknown a priori, the challenge is how to study the multiple time-scale problem (adiabatic and nonadiabatic processes) of the nonequilibrium system dynamics.

In this paper we show, through mathematical transformation, that the coupled nonequilibrium landscapes become equivalent to a single landscape but with additional degrees of freedom: Intra- and interlandscape motion on the coupled landscapes become motion along the multidimensional surface of the unique landscape. On this single landscape, dynamics can be decomposed to two determining factors: the gradient of the potential landscape, which is closely related to the steady-state probability distribution of the enlarged dimensions, and the probability flux, which has the curl nature. We have summarized the approach in Fig. 1. Fig. 1*A* shows the equilibrium adiabatic dynamics, which is determined by the gradient of the single energy landscape known a priori. Fig. 1*B* shows the nonequilibrium adiabatic dynamics determined by both gradient and curl flux on the single nonequilibrium landscape (2). Fig. 1*C* shows the nonadiabatic multiple equilibrium landscape surfaces with the known energy function of each individual surface where the dynamics is determined by the combination of the gradient of the surface and hopping between surfaces, which has been traditionally the focus

Author contributions: M.S. and J.W. designed research; K.Z., M.S., and J.W. performed research; M.S. and J.W. contributed new reagents/analytic tools; K.Z., M.S., and J.W. analyzed data; and M.S. and J.W. wrote the paper.

The authors declare no conflict of interest.

This article is a PNAS Direct Submission.

[1]To whom correspondence may be addressed. E-mail: sasai@cse.nagoya-u.ac.jp or jin.wang.1@stonybrook.edu.

This article contains supporting information online at www.pnas.org/lookup/suppl/doi:10.1073/pnas.1305604110/-/DCSupplemental.

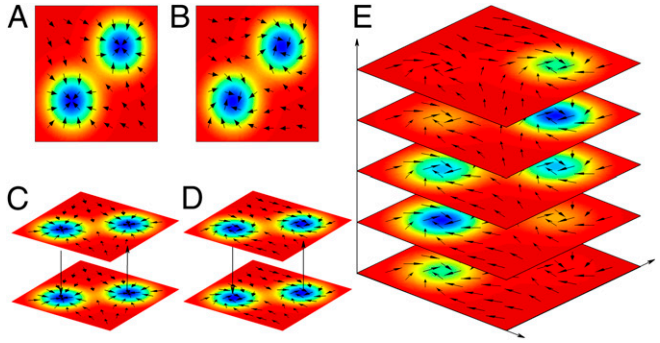

Fig. 1. Illustrations of the equilibrium/nonequilibrium and adiabatic/nonadiabatic landscapes. (*A*) The adiabatic single landscape that underlies the equilibrium gradient dynamics. (*B*) The adiabatic single landscape that underlies the nonequilibrium dynamics determined by both the landscape gradient and curl flux. (*C*) The nonadiabatic multiple landscapes where the dynamics is determined by the combination of the gradient of the individual landscape and hopping between the landscapes. (*D*) The nonadiabatic multiple landscapes where dynamics is determined by both the landscape gradient and curl flux as well as the additional interlandscape hopping. (*E*) The description equivalent to *D* with the single landscape for nonadiabatic nonequilibrium systems in the continuous representation, where the dynamics is determined by the gradient of the landscape and curl flux or eddy current on the expanded space.

of studies on nonadiabaticity (1). Fig. 1*D* shows nonadiabatic, multiple nonequilibrium landscapes without energy function a priori known. The nonadiabatic dynamics is determined by both gradient and curl flux along each landscape as well as the additional interlandscape hopping. In the context of gene switching, this coupled intra- and interlandscape dynamics has been referred to as "eddy" or "churn" (19). Finally Fig. 1*E* shows the equivalent description of Fig. 1*D*, in which nonadiabatic dynamics is described with a single landscape by expressing the eddy current as the curl flux in the expanded dimensions.

The more general stochastic case can be described by the discrete processes such as molecular number changes rather than a continuous process such as concentration changes. Our starting point is the general discrete process in this study. As seen, when the molecular number is sufficiently large, the discrete picture with molecular numbers emerges to the continuous picture with concentrations. An important example is a self-regulating gene circuit, which has two landscapes for the gene off and on states and the motion along each landscape quantifies the protein concentration change. We show in this paper that eddy current has dramatic effects on this system: (*i*) the broadening of the basin of attraction through nonadiabatic skewing, (*ii*) irreversibility of the kinetic paths, (*iii*) increased amplitude of noise, (*iv*) emerging oscillatory component in relaxation, (*v*) time reversal symmetry breaking in three-point correlation function, and (*vi*) entropy production and dissipation raised from the nonadiabatic condition. These properties are essential for quantifying the nonequilibrium complex system dynamics.

The eddy current and landscape framework developed here is easy to visualize for the underlying physical process and can be used to guide further investigation of the physical and biological nonequilibrium systems.

Theory for Nonequilibrium Eddy Current

To illustrate the concepts and the methods, we here focus on the simplest case that the system has two landscapes labeled with $s=0$ or 1 and a one-dimensional continuous variable ψ that represents the motion along individual landscapes. See *Materials and Methods* for more general cases of N landscapes with M dimensions. We consider $P_0(\psi)$ and $P_1(\psi)$, the probability density at ψ in the landscapes of $s=0$ and $s=1$, respectively, with the normalization $\int d\psi \sum_{s=0}^{1} P_s(\psi)=1$. As explained in *Materials and Methods* and *SI Text*, this $N=2$ and $M=1$ problem is converted to the $M+1$ dimensional single landscape problem by using the method similar to the coherent-state representation of a quantum spin: Considering the probability to select two landscapes, $\cos^2(\theta/2)$ and $\sin^2(\theta/2)$, $P_s(\psi)$ can be written as $P_1(\psi)=\int \sin\theta\, d\theta(\cos^2(\theta/2))P_\theta(\psi)$ and $P_0(\psi)=\int \sin\theta\, d\theta(\sin^2(\theta/2))P_\theta(\psi)$. Then, the problem is to determine the 2D distribution $P_\theta(\psi)$ in the θ–ψ space. We apply this method of the coherent-state representation to a circuit of a self-regulating gene.

Example Self-Regulating Gene. Dynamics of the self-regulating gene shown in Fig. 2*A* can be described by the DNA state, which we represent as $s=1$ and 0, and the copy number of protein, n. When the regulator protein is an activator (repressor), the gene is on (off) upon its binding to DNA. When the gene is on, through transcription and translation the protein is actively synthesized. In the self-regulating gene system, the protein produced by the gene will act back to its own gene. The dynamics of such a system can be described by the underlying chemical reactions for protein synthesis and degradation, and the binding/unbinding of the regulating protein to DNA. Because there are only a finite number of molecules (typically $n<10^4$) in a cell, the statistical fluctuations in n need to be taken into consideration. The system dynamics can be thus described by the following master equation:

$$\begin{aligned}\frac{\partial \mathbf{P}(n)}{\partial t} &= \begin{pmatrix} g_1 & 0 \\ 0 & g_0 \end{pmatrix}[\mathbf{P}(n-1)-\mathbf{P}(n)] \\ &+k(n+1)\mathbf{P}(n+1)-kn\mathbf{P}(n) \\ &+\begin{pmatrix} -h(n) & f \\ h(n) & -f \end{pmatrix}\mathbf{P}(n).\end{aligned} \quad [1]$$

Here, $\mathbf{P}(n)$ is a vector with two components, $P_1(n)$ and $P_0(n)$, and $P_s(n)$ is the probability of the protein-copy number n in the DNA state with the regulator protein unbound $(s=1)$ or bound $(s=0)$. g_s is the synthesis rate of protein at the DNA state s. $g_1>g_0$ for the self-repressor and $g_1<g_0$ for the self-activator case. k is the degradation rate constant of the protein. h is the

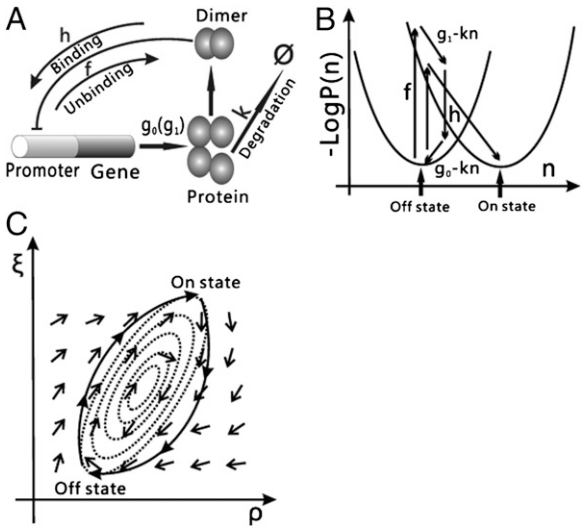

Fig. 2. Illustrations of self-regulating gene dynamics. (*A*) Reaction scheme in the self-regulating gene circuit. (*B*) The multiple landscapes and dynamics of the self-regulating gene based on the view of Fig. 1*D* (dimension of individual landscapes is one in *B* and two in Fig. 1*D*). Two parabolas are landscapes at the gene off and on states and vertical arrows are hopping between landscapes. (*C*) The equivalent single landscape and dynamics on the expanded space of the protein concentration ρ and the gene state ξ. Dotted lines show the basin of attractor and arrows represent the curl flux.

binding rate of the regulator protein to DNA and f is the unbinding rate of the regulator protein from DNA. We assume that the regulator is a dimer of the product protein, so that $h(n) = h_0 n(n-1)$ with a rate coefficient h_0. The important dimensionless parameter is

$$\omega = f/k, \qquad [2]$$

which is the adiabaticity parameter. When ω is large, the binding/unbinding of the proteins to/from DNA is much faster than the synthesis and degradation of the protein; the system is in the adiabatic limit. When ω is small, the binding/unbinding of the protein to/from DNA is comparable to or slower than the protein-copy number change; the system is in the nonadiabatic regime. The ω parameter characterizes the relative dynamic time scales of the system and will be the focus of our discussion, as mentioned earlier.

Because the discrete variable n is typically $n \gg 1$, it is convenient to transform it to a continuous variable ψ by expanding $P_s(n)$ with bases of the Poisson distribution functions as $P_s(n) = \int d\psi P_s(\psi)\overline{P}(n,\psi)$, where $\overline{P}(n,\psi)$ is the Poisson distribution of n at around the average ψ, and $P_s(\psi)$ is the weight distribution on the sth landscape. In this way we can regard the self-regulating gene dynamics as an s–ψ problem of coupled landscapes with $N = 2$ and $M = 1$. As mentioned, the global physical principle of this kind of dynamics on the coupled landscapes is challenging to describe despite the computational efforts. We will solve this issue by transforming the representation of discrete on and off states of the gene into the continuous representation.

For the convenience of our mathematical transformation, we write Eq. **1** in the conventional quantum mechanical second quantized form (17, 25) by following the method of Doi (26, 27) and Peliti (28). Then, the master equation can be exactly transformed into the path-integral form by using the coherent-state representation of Eq. **7** and the identify of Eq. **8** in *Materials and Methods*. With this path-integral representation, the transition probability between the states of different protein-copy numbers is expressed by the functional of $\theta(t)$ and $\psi(t)$ and their conjugate auxiliary variables $\phi(t)$ and $\chi(t)$. When we expand the functional in terms of ϕ and χ and retain up to the second-order terms, that is, to take the Gaussian approximation (29), then the problem is transformed into the $M+1$ dimensional θ–ψ problem. With this approximation, the coupled Langevin equations are derived for $\xi = \cos\theta$ and $\rho = \psi/\Omega_0$, with Ω_0 being the system volume, as

$$\dot{\rho} = -\rho + x^{ad} + \xi\delta x + \epsilon_\rho \qquad [3]$$

$$\frac{1}{\omega}\dot{\xi} = -\kappa(1+\xi)\rho^2 + (1-\xi) + \epsilon_\theta, \qquad [4]$$

with

$$<\epsilon_\rho(t)\epsilon_\rho(t')> = \frac{1}{\Omega_0}\left(\rho + x^{ad} + \xi\delta x\right)\delta(t-t'),$$

$$<\epsilon_\theta(t)\epsilon_\theta(t')> = \frac{2}{\omega}\left(\kappa(1+\xi)\rho^2 + (1-\xi)\right)\delta(t-t').$$

Here, t in Eqs. **3** and **4** is normalized by the unit of $1/k$. $x^{ad} = (g_1+g_0)/(2k\Omega_0)$ is the typical value of the protein concentration, $\delta x = (g_1-g_0)/(2k\Omega_0)$ is the difference in the typical protein concentration between the gene on and off states, and $\kappa = h_0\Omega_0^2/f$ mimics the equilibrium binding constant of the protein to DNA. Notice that ξ is an experimentally observable quantity with $(1+\xi(t))/2$ being the probability that the gene is on and $(1-\xi(t))/2$ being the probability that the gene is off at a given time instance.

ρ in Eq. **3** represents the protein concentration, so that Eq. **3** is a usual Langevin equation of the large volume Ω expansion, representing the statistical fluctuations due to the finite number of molecules, and we can write that Eq. **4** is the corresponding equation of the adiabaticity parameter ω expansion, representing the time-scale fluctuations deviating from the adiabatic case.

To obtain quantitatively more reliable results, we can further extend the present method by using the distribution of the form $P_\theta(\psi_1,\psi_0)$ including more variables instead of $P_\theta(\psi)$ used here. See *SI Text* for the explicit derivation of Eqs. **3** and **4** and their extension.

Adiabatic Limit. In the strong adiabatic limit of $\omega \to \infty$, both the left-hand side of Eq. **4** and the noise term tend to zero because they are inversely proportional to the ω and $\sqrt{\omega}$, respectively. As a result, we can see that Eq. **4** turns to $-\kappa(1+\xi)\rho^2 + (1-\xi) = 0$ or $\xi = \frac{1-\kappa\rho^2}{1+\kappa\rho^2}$. If we substitute this expression to Eq. **3**, we get $\dot{\rho} = -\rho + x^{ad} + \frac{1-\kappa\rho^2}{1+\kappa\rho^2}\delta x + \epsilon_\rho$ or equivalently $\dot{\rho} = -\frac{\partial U}{\partial \rho} + \epsilon_\rho$, where U is the effective potential given as $U = \frac{1}{2}\rho^2 - x^{ad}\rho - \delta x\left(\frac{2\arctan[\sqrt{\kappa}\rho]}{\sqrt{\kappa}} - \rho\right)$. Therefore, for the self-regulating gene in the adiabatic limit, due to the strong interactions causing frequent flipping of the gene states, we reduce this to a one-dimensional problem. Because of the one-dimensional nature of the problem, dynamics is represented as a pure gradient dynamics with an effective potential landscape U.

Extreme Nonadiabatic Limit. In the extreme nonadiabatic condition of $\omega \to 0$, Eq. **4** becomes $\dot{\xi} = 0$ so that $\xi = const.$ and the motion is fixed at a specific ξ along ρ. Again, the effective dynamics is a gradient of the potential landscape along one-dimensional protein concentration coordinates ρ with effective potential $U = \frac{1}{2}\rho^2 - (x^{ad} + \xi\delta x)\rho$. There is essentially no jumping between the energy surfaces because the binding/unbinding of regulators to DNA is so slow. Therefore, the dynamics becomes very simple, following the gradient of the potential along a single energy landscape surface without any curl flux component. In this way, for both extreme cases of fast or slow binding/unbinding of proteins to DNA relative to the synthesis and degradation of the proteins, the dynamics of the self-regulator is driven by the pure gradient of the underlying single potential landscape.

Potential and Curl Flux in the Moderate Nonadiabatic Regime. If ω is not necessarily large, that is, in the moderately nonadiabatic regime, we do not have the time-scale separation any more as in the adiabatic or nonadiabatic limit, and hence there is no approximation we can use for simplifying Eqs. **3** and **4** further. Therefore, the system is inherently two dimensions. In this case, we can write down the corresponding Fokker–Planck equation as the probability conservation with the local change of the probability due to the incoming or outgoing 2D flux:

$$\partial P/\partial t = -\nabla\cdot\mathbf{J} = -\nabla\cdot[\mathbf{F}P - (1/2)\nabla\cdot(\mathbf{D}P)]. \qquad [5]$$

Here, the driving force $\mathbf{F}$ and the diffusion matrix $\mathbf{D}$ are derived from Eqs. **3** and **4**. We can explore the steady-state probability distribution $P_{ss} = P(t\to\infty)$ from $\partial P_{ss}/\partial t = -\nabla\cdot\mathbf{J}_{ss} = 0$. Thus, the steady-state probability flux $\mathbf{J}_{ss}$ is divergent-free and is written as $\mathbf{J}_{ss} = \mathbf{F}P_{ss} - 1/2\,\nabla\cdot(\mathbf{D}P_{ss})$. Then, using the population potential $U = -\ln P_{ss}$, the driving force $\mathbf{F}$ can be decomposed into three terms: $\mathbf{F} = -1/2\,\mathbf{D}\cdot\nabla U + \mathbf{J}_{ss}/P_{ss} + 1/2\,\nabla\cdot\mathbf{D}$. Because the third term can be absorbed to the total driving force, the main components of the driving force are $-\mathbf{D}\cdot\nabla U$ and $\mathbf{J}_{ss}/P_{ss}$.

In the equilibrium system, unlike the present example genetic system, we have $\mathbf{J}_{ss} = 0$, so that there is no net flux and the detailed balance is preserved. The corresponding dynamics is determined by the force from the gradient of the potential. In the nonadiabatic case, as in the present example system, $\mathbf{J}_{ss} \neq 0$ and $\mathbf{J}_{ss}$ depends on the system variables. Therefore, the detailed balance is broken and the system becomes nonequilibrium. The divergent free $\mathbf{J}_{ss}$ has no sources or sinks to start or end up, so that $\mathbf{J}_{ss}$ has a curl rotating nature. In this nonadiabatic case, where the detailed balance is broken explicitly, the degree of

nonequilibriumness or detailed balance breaking is quantified by the strength of $\mathbf{J}_{ss}$. So, in the 2D space of ρ and ξ in the nonadiabatic regime, the dynamics is determined by both the gradient of the landscape U and the curl flux. Instead of straightly going down to the gradient, the motion proceeds curly-spiraling down the gradient.

In the conventional view, the self-regulating gene system is described by two landscapes each in ρ space with the discrete gene-state labeling of $\xi = -1$ and $\xi = 1$. In the nonadiabatic regime, stochastic dynamics mainly moves along one landscape and occasionally jumps to another landscape. Moving along the new landscape for a while, then the system jumps back to the original landscape. This process keeps on iterating, so the stochastic trajectory along and between the two landscapes forms a cyclic churn- or eddy-like spiraling motion (Fig. 2*B*). In the present view, although dynamics along the specific gene state can be determined by the gradient of the single potential surface, the motion in the 2D space of ρ and ξ can no longer be seen in this way. In fact, the dynamics can be described by a single potential landscape U instead of two individual landscapes, giving the gradient part of the dynamics, and the curl probability flux provides the origin of the eddy current motion in dynamic trajectories (Fig. 2*C*). From this continuous representation, we can quantify the origin of the eddy current motion found in simulations by the strengths of the curl steady-state probability flux.

We must point out that for general complex dynamical systems with $M \geq 2$, even in the adiabatic limit of time-scale separation, the dynamics in general is not driven by a pure gradient of a single potential landscape but in addition a curl flux force. The origin of this curl is from the underlying dynamics on the adiabatic landscape. However, in the nonadiabatic regime, the curl flux has two contributions, one from the adiabatic part and the other from the nonadiabatic part with the time-scale consideration (Fig. 1*E*).

Eddy Current in a Self-Repressing Gene. The curl flux leading to the eddy current brings about the dramatic effects on the self-regulating gene dynamics. Here, these effects are analyzed by solving Eqs. **3** and **4** numerically for the self-repressing case.

Shown in Fig. 3 are 2D contour maps of the probability landscape $U = -\ln P_{ss}$ in the protein concentration ρ and the gene state ξ. The landscape has a single basin of attraction. When the ω is large, the orientation of landscape is vertical and therefore the corresponding projections to the protein-concentration variable at the two gene states of $\xi = -1$ and $\xi = 1$ give the same result at the same location. Therefore, only a single peak for the distribution at the protein concentration space is expected. However, when the ω becomes smaller, the landscape still has a single basin of attraction, but the orientation of the landscape is tilted. The smaller the ω is, the more tilted the landscape is. This leads to the corresponding projections to the protein concentration variable at $\xi = -1$ and $\xi = 1$ giving the different results at the two different locations. Therefore, two peaks for the distribution at the protein concentration space are expected when ω is small in the nonadiabatic regime, which is the possibility ignored in the conventional view of gene switches (9–21). Fig. S1 shows the calculated two-peak distribution for the low ω. The two peaks of the protein concentration distribution, therefore, are originated from the tilted landscape, which breaks the symmetry of the original one-peak distribution.

Arrows superimposed in Fig. 3 are fluxes $\mathbf{J}_{ss}$ curling around the basin, and lines in Fig. 3 are the dominant kinetic paths (kinetic paths with the largest weight) from the gene on state to the off state and back, which are quantitatively obtained using our path integral method for nonequilibrium systems (4). When the ω is large, the orientation of the landscape is vertical and the forward and the backward dominant kinetic paths are almost identical and opposite in direction, which is expected because the underlying dynamics is driven by the gradient of the potential landscape. Therefore, J_{path}, which is the integration of $\mathbf{J}_{ss}$ along a circle or closed loop of the dominant kinetic paths, is negligibly small. However, when the ω becomes smaller, the orientation of the landscape is tilted. Then, the forward and backward dominant kinetic paths are significantly different from each other, and J_{path} becomes large. J_{path}, therefore, is a measure of the effective strength of curl flux or eddy current and is plotted in Fig. 4*A* as a function of ω. Increase of curl flux J_{path} in small ω shows the irreversibility of the dominant kinetic paths and implies the violated time-reversal symmetry.

The distribution width of protein concentration is quantified in Fig. 4*B*. We found that when curl flux is small and the ω is large, the binding/unbinding is frequent, and therefore the gene states are strongly coupled. This leads to the narrower Poisson distribution (Fano factor equal to 1) of the peak in the distribution of protein concentration, that is, because the dynamics essentially follows the gradient of the effective landscape and motion is convergent to the same location. However, when curl flux is large and the ω is smaller, the coupling between the gene states is weaker. The large curl flux will increase the dispersion of the motion, leading the distribution of the protein concentration to split from one peak to two peaks. We see the broader non-Poisson distribution (Fano factor significantly larger than 1) of the protein concentration with the intense curl flux.

The curl flux breaks the detailed balance and gives irreversibility. This irreversibility is evident in the higher-order correlation function. In Fig. 4*C*, we calculated the difference between the forward and backward three-point correlation functions in time as

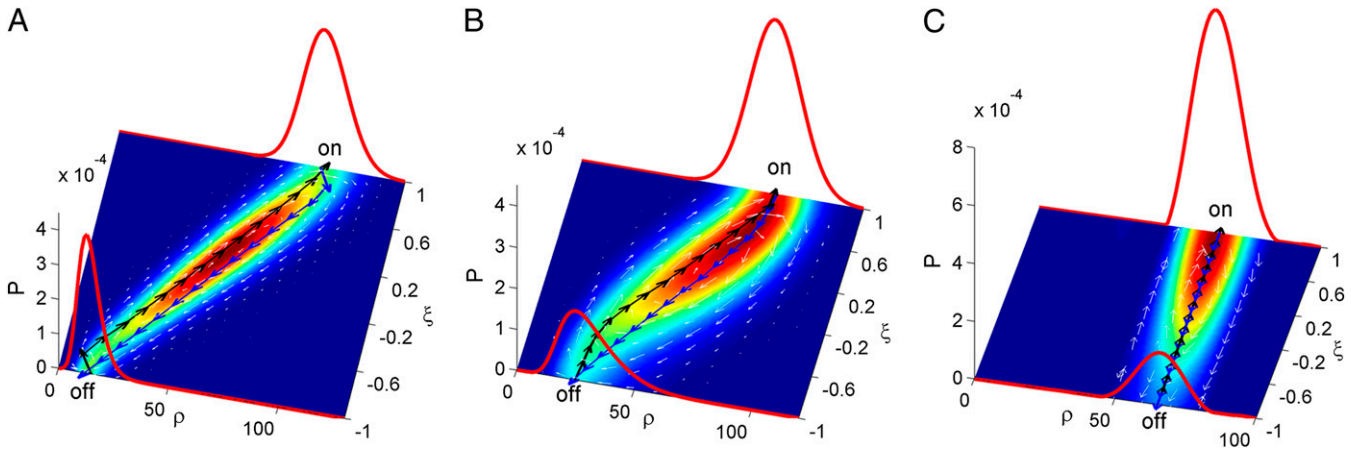

Fig. 3. Calculated single composite landscape on the expanded space of the protein concentration ρ and the gene state ξ at (*A*) $\omega = 0.01$, (*B*) $\omega = 0.1$, and (*C*) $\omega = 100$. Superimposed on the landscape are $\mathbf{J}_{ss}$ (white arrows) and the dominant kinetic paths between the gene on and off states (black lines and blue lines). Red lines are distributions of ρ in the gene off ($\xi = -1$) and on ($\xi = 1$) states.

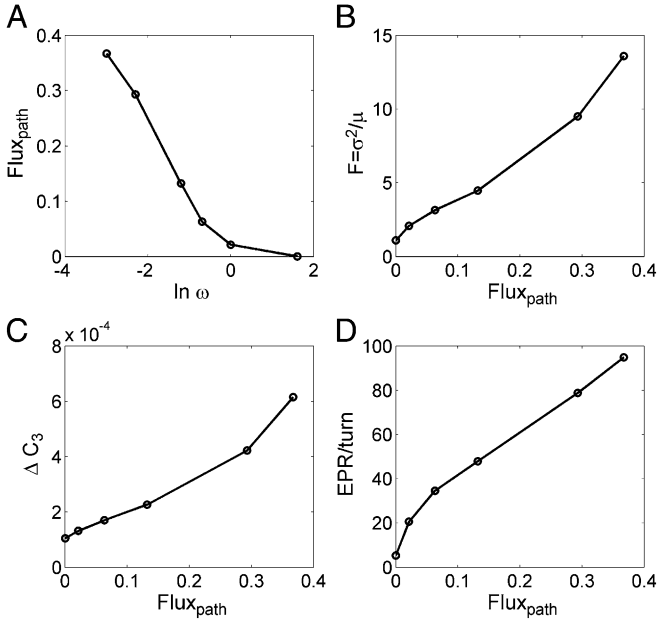

Fig. 4. Anomalies arising from the nonadiabatic curl flux in the self-repressing gene. Quantities calculated from the Langevin equations for ρ and ξ are plotted. (*A*) The effective strength of curl flux J_{path} is anticorrelated with ω and largely increases in the nonadiabatic regime of $\omega < 1$. (*B*) The Fano factor, which is the variance divided by the mean, showing the relative width of the steady-state probability distribution of protein concentration, (*C*) difference between the forward and backward three-point correlation functions of protein concentration, and (*D*) the entropy production per turn of the on/off gene switching are plotted as functions of J_{path}, showing that these quantities are correlated with curl flux.

$$\Delta C_3 = \int_{t_1 \geq 0} dt_1 \int_{t_2 \geq 0} dt_2 (C_3(t_1, t_2) - C_3(-t_1, -t_2))^2,$$

with

$$C_3(t_1, t_2) = \langle \delta\rho(\tau)\delta\rho(\tau + t_1)\delta\rho(\tau + t_1 + t_2)\rangle / \langle \delta\rho^2 \rangle^{3/2},$$

where $\delta\rho(t)$ is the fluctuation of the protein concentration, $\delta\rho(t) = \rho(t) - \langle\rho\rangle$. We found ΔC_3 is small for small curl flux. This is because for the adiabatic case the detailed balance is effectively preserved, which leads to this time symmetry. However, for the nonadiabatic case of large curl flux, the dynamics of the system is driven by the gradient of the potential landscape and in addition the curl flux. We can see ΔC_3 becomes larger as the curl flux increases in small ω. The three-point correlation function can be measured experimentally, which should provide a direct probe to the effect of the curl flux (30, 31).

The curl flux manifests itself also in the oscillatory behavior of the gene dynamics. As shown in Fig. S2, the two-time correlation function $C_2(t) = \langle \delta\rho(\tau)\delta\rho(\tau + t)\rangle / \langle \delta\rho^2 \rangle$ apparently starts to have oscillations when ω is smaller. Also shown in Fig. S2 are Fourier transform spectra of the two-time correlation functions, which show the Lorentzian-like curve at large ω but are peaked at small ω, implying oscillation. The curling nature of the flux is the origin of this oscillation, so that the complexity in the time correlation function deviating from single exponential or the peaked power spectrum deviating from Lorentzian is a quantitative signature of the curl flux and detailed balance breaking.

In Fig. 4*D*, we plot the entropy production during a cycle of on–off switching, which was calculated by normalizing the average entropy production rate R_S by a typical turnover time for switching $\sim 1/\omega$ as R_S/ω. R_S is the product of the potential gradient and the curl flux analogous to voltage and electric current in an electrical circuit, which gives dissipation. We found the entropy production per switching is nearly zero in the adiabatic regime where the curl flux is small. This is because in the adiabatic regime the system is in effective equilibrium state without significant curl flux. This leads to the effective zero entropy production rate per switching. However, the entropy production increases as curl flux increases. When the flux in and out of the system owing to the energy, entropy, or material exchange becomes larger, the dissipation is naturally larger, analogous to increasing the current in an electric circuit leading to more thermal dissipations. Again the curl flux is the origin of the entropy production or dissipations.

Quantities shown in Fig. 4 and Figs. S1 and S2, the shape and width of the protein concentration distribution, the two-point and three-point correlations, and dissipations in gene switching are experimentally measurable quantities, which should highlight the eddy-current effects in experimental observations.

Summary and Discussion

In this work, we have established a theoretical framework to study the nonadiabatic nonequilibrium dynamics of complex systems, or in other words, the nonequilibrium dynamics with the dynamical time scales involved. Whereas the nonequilibrium complex systems are often dictated by both the single landscape gradient and curl flux, the nonadiabatic dynamics is typically involved with time scales, which gives multiple landscapes. The challenge is how to incorporate both natures into one unified picture. We have found this problem can be equivalently quantified by the dynamics in a single landscape with expanded dimensions. The nonadiabatic motion from dynamical time scales can give the nonzero curl flux in this expanded space, leading to detailed balance breaking. Fig. 1 gives a summary of the previous (Fig. 1 *A–D*) and our unified (Fig. 1*E*) approaches.

We investigated the effects of the curl flux caused by the nonadiabaticity of the dynamic time scales. We found that this nonzero curl flux can give rise to eddy current with curling motions. Specifically, Fig. 4 implies that the nonadiabaticity owing to the time scales gives the emergence of the extra dimensionality (different landscapes) and is the source of the flux from the extra dimension to the original system. The nonzero flux is the source of the spread of protein concentration distribution, the irreversibility measured by the three-point correlation functions, and the dissipation cost. The nonzero flux provides the possibility of multiple states owing to curling and stretching and the two-point correlation function reveals the time-scale complexity of the resulting multiple states.

In most previous studies, gene switches have been analyzed under the assumption of the adiabatic limit (32). Although this assumption should be reasonable for many bacterial switches in which gene switching is regulated by the fast binding/unbinding of repressors or activators to/from DNA, this approximation should not hold true in the complex gene switches of eukaryotes. Indeed, in embryonic stem cells derived from early mammalian embryos, the two-peak distribution of the expression level of a key factor protein Nanog has been observed. Individual cells strongly oscillate to bring about dynamical fluctuations between the two states having the different Nanog expression strength (33, 34). Another factor of embryonic stem cell, Hes1, shows a clear oscillation pattern in the expression level (35). These data suggest the dynamical time scales of gene switches are essential to understand cell biology of higher organisms. It is important to examine whether the concepts and techniques developed in this paper are applicable to those problems of eukaryotic gene switches. It is straightforward to extend the present results to cases in which multiple genes are coupled to form a network. We expect that the eddy current or the nonadiabatic curl flux in the gene network decisively affects cell behavior. We expect that our general theoretical framework can be applied to many physical and biological processes where the underlying dynamics is either in equilibrium or nonequilibrium involving dynamic time scales.

Materials and Methods

Consider the case that the system has a discrete variable s that can take the value from 0 to $N-1$, and a set of M continuous variables $\hat{\psi}$. The system, therefore, has N landscapes with M dimensions, where the change in s quantifies the hopping between landscapes and the change in $\hat{\psi}$ quantifies the motion along individual landscapes. We here describe the idea of the coherent-state representation to transform s into a continuous variable θ.

By defining a vector $\langle s| = (0,\ldots,1,\ldots,0)$ whose sth component is 1 but other $N-1$ components are 0, and $|s\rangle = \langle s|^T$, where ^{T} represents transpose, the probability density at $\hat{\psi}$ in the sth landscape, $P_s(\hat{\psi})$, can be represented in a vector form as $\mathbf{P}(\hat{\psi}) = \sum_s P_s(\hat{\psi})|s\rangle$. In analogy with the coherent-state representation of a quantum spin, $\{|s\rangle\}$ can be transformed to the basis set $\{|\Omega\rangle\}$ as

$$\mathbf{P}(\hat{\psi}) = \int d\Omega P_\Omega(\hat{\psi})|\Omega\rangle, \qquad [6]$$

where $\Omega = (\theta,\phi)$ is the solid angle, $\int d\Omega = \frac{1}{4\pi}\int_0^{2\pi} d\phi \int_0^{\pi} \sin\theta\, d\theta$, and $\{|\Omega\rangle\}$ and $\{|s\rangle\}$ are related to each other by

$$|\Omega\rangle = \sum_{s=0}^{N-1} {}_{N-1}C_s \left(u(\theta)e^{i\phi/2}\right)^s \left(v(\theta)e^{-i\phi/2}\right)^{N-1-s}|s\rangle, \qquad [7]$$

with ${}_{N-1}C_s = (N-1)!/(s!(N-1-s)!)$, $u(\theta) = \cos^2(\theta/2)$, and $v(\theta) = \sin^2(\theta/2)$. By introducing a conjugate vector, $\langle\hat{\Omega}| = Ne^{i\phi(N-1)/2}\sum_{s=0}^{N-1} e^{-is\phi}\langle s|$, we have the relation

$$\int d\Omega|\Omega\rangle\langle\hat{\Omega}| = \sum_{s=0}^{N-1}|s\rangle\langle s| = 1, \qquad [8]$$

which shows $\{|\Omega\rangle\}$ is an overcomplete basis set. Notice that unlike the usual expression for quantum spins, $|\Omega\rangle$ and $\langle\hat{\Omega}|$ are not Hermite conjugate of each other, but this representation was chosen here to reflect the constraint to normalize the probability distribution (*SI Text*). As shown explicitly in the example of gene switching in the section *Example Self-Regulating Gene*, ϕ plays a role of an auxiliary variable to determine the fluctuation width of θ. In this way, the original s–$\hat{\psi}$ problem, that is, the N landscape problem, is transformed into the θ–$\hat{\psi}$ problem, that is, the single landscape problem of $M+1$ dimensions.

It should be noted that when the system is composed of K subsystems (K genes, for example), the system should have NK landscapes represented by K variables $s_1, s_2, \ldots, s_K$, each of which can take a value from 0 to $N-1$. Then, through the coherent-state representation explained above, the system is described by K continuous variables $\theta_1, \theta_2, \ldots, \theta_K$ and the M dimensional variable, $\hat{\psi}$, so that the problem is converted to the $M+K$ dimensional single-landscape problem. Extensions to the further complex cases are straightforward.

Eq. **7** is particularly simple when $N=2$ as $|\Omega\rangle = u(\theta)e^{i\phi/2}|1\rangle + v(\theta)e^{-i\phi/2}|0\rangle$. Combining with Eq. **6**, we have $\mathbf{P}(\hat{\psi}) = \int \sin\theta\, d\theta(\cos^2(\theta/2)P^1_\theta(\hat{\psi})|1\rangle + \sin^2(\theta/2)P^0_\theta(\hat{\psi})|0\rangle)$, with $P^1_\theta(\hat{\psi}) = \int \frac{d\phi}{2\pi} P_\Omega(\hat{\psi})e^{i\phi/2}$ and $P^0_\theta(\hat{\psi}) = \int \frac{d\phi}{2\pi} P_\Omega(\hat{\psi})e^{-i\phi/2}$. When $P_\Omega(\hat{\psi})$ has a Gaussian distribution at around $\phi = 0$, we can put $P^1_\theta(\hat{\psi}) = P^0_\theta(\hat{\psi}) = P_\theta(\hat{\psi})$, with which the notions used in the section *Theory for Nonequilibrium Eddy Current* are obtained.

ACKNOWLEDGMENTS. This work was supported by National Science Foundation of China Grants 21190040 and 11174105, and 973 Project Grants 2009CB930100 and 2010CB933600 (to K.Z.); and Japan Society for the Promotion of Science Grants-in-Aid for Scientific Research 24244068 and 23654147 (to M.S.). J.W. thanks the National Science Foundation for support.

1. Marcus RA, N. Sutin N (1985) Electron transfers in chemistry and biology. *Biochim Biophys Acta* 811(3):265–322.
2. Wang J, Xu L, Wang E (2008) Potential landscape and flux framework of nonequilibrium networks: Robustness, dissipation, and coherence of biochemical oscillations. *Proc Natl Acad Sci USA* 105(34):12271–12276.
3. Wang J, Xu L, Wang EK, Huang S (2010) The potential landscape of genetic circuits imposes the arrow of time in stem cell differentiation. *Biophys J* 99(1): 29–39.
4. Wang J, Zhang K, Wang EK (2010) Kinetic paths, time scale, and underlying landscapes: A path integral framework to study global natures of nonequilibrium systems and networks. *J Chem Phys* 133(12):125103.
5. Feng H, Wang J (2011) Potential and flux decomposition for dynamical systems and non-equilibrium thermodynamics: Curvature, gauge field, and generalized fluctuation-dissipation theorem. *J Chem Phys* 135(23):234511.
6. Wang J, Zhang K, Xu L, Wang EK (2011) Quantifying the Waddington landscape and biological paths for development and differentiation. *Proc Natl Acad Sci USA* 108(20): 8257–8262.
7. Zhang F, Xu L, Zhang K, Wang EK, Wang J (2012) The potential and flux landscape theory of evolution. *J Chem Phys* 137(6):065102.
8. Ao P (2004) Potential in stochastic differential equations: Novel construction. *J Phys Math Gen* 37(3):L25–L30.
9. Hornos JEM, et al. (2005) Self-regulating gene: An exact solution. *Phys Rev E Stat Nonlin Soft Matter Phys* 72(5 Pt 1):051907.
10. Kim KY, Wang J (2007) Potential energy landscape and robustness of a gene regulatory network: Toggle switch. *PLOS Comput Biol* 3(3):e60.
11. Kim KY, Lepzelter D, Wang J (2007) Single molecule dynamics and statistical fluctuations of gene regulatory networks: A repressilator. *J Chem Phys* 126(3):034702.
12. Lepzelter D, Kim KY, Wang J (2007) Dynamics and intrinsic statistical fluctuations of a gene switch. *J Phys Chem B* 111(34):10239–10247.
13. Schultz D, Ben Jacob E, Onuchic JN, Wolynes PG (2007) Molecular level stochastic model for competence cycles in *Bacillus subtilis*. *Proc Natl Acad Sci USA* 104(45): 17582–17587.
14. Yoda M, Ushikubo T, Inoue W, Sasai M (2007) Roles of noise in single and coupled multiple genetic oscillators. *J Chem Phys* 126(11):115101.
15. Feng H, Han B, Wang J (2011) Adiabatic and non-adiabatic non-equilibrium stochastic dynamics of single regulating genes. *J Phys Chem B* 115(5):1254–1261.
16. Feng H, Han B, Wang J (2012) Landscape and global stability of nonadiabatic and adiabatic oscillations in a gene network. *Biophys J* 102(5):1001–1010.
17. Sasai M, Wolynes PG (2003) Stochastic gene expression as a many-body problem. *Proc Natl Acad Sci USA* 100(5):2374–2379.
18. Walczak AM, Sasai M, Wolynes PG (2005) Self-consistent proteomic field theory of stochastic gene switches. *Biophys J* 88(2):828–850.
19. Walczak AM, Onuchic JN, Wolynes PG (2005) Absolute rate theories of epigenetic stability. *Proc Natl Acad Sci USA* 102(52):18926–18931.
20. Okabe Y, Yagi Y, Sasai M (2007) Effects of the DNA state fluctuation on single-cell dynamics of self-regulating gene. *J Chem Phys* 127(10):105107.
21. Shi P-Z, Qian H (2011) A perturbation analysis of rate theory of self-regulating genes and signaling networks. *J Chem Phys* 134(6):065104.
22. Wang H, Oster G (2002) Ratchets, power strokes, and molecular motors. *Appl Phys, A Mater Sci Process* 75(2):315–323.
23. Schief WR, Howard J (2001) Conformational changes during kinesin motility. *Curr Opin Cell Biol* 13(1):19–28.
24. Zhang X-J, Qian H, Qian M (2012) Stochastic theory of nonequilibrium steady states and its applications. Part I. *JPhys Rep* 510(1-2):1–86.
25. Mattis DC, Glasser ML (1998) The uses of quantum field theory in diffusion-limited reactions. *Rev Mod Phys* 70(3):979–1001.
26. Doi M (1976) Second quantization representation for classical many-particle system. *J Phys Math Gen* 9(9):1465–1477.
27. Doi M (1976) Stochastic theory of diffusion-controlled reaction. *J Phys Math Gen* 9(9): 1479–1495.
28. Peliti L (1985) Path integral approach to birth-death processes on a lattice. *J Phys* 46(9):1469–1483.
29. Itakura K, Ohkubo J, Sasa S-I (2010) Two Langevin equations in the Doi-Peliti formalism. *J Phys A Math Theor* 43(12):125001.
30. Qian H, Elson EL (2004) Fluorescence correlation spectroscopy with high-order and dual-color correlation to probe nonequilibrium steady states. *Proc Natl Acad Sci USA* 101(9):2828–2833.
31. Li CH, Wang EK, Wang J (2011) Landscape, flux, correlation, resonance, coherence, stability, and key network wirings of stochastic circadian oscillation. *Biophys J* 101(6): 1335–1344.
32. Tkačik G, Walczak AM (2011) Information transmission in genetic regulatory networks: A review. *J Phys Condens Matter* 23(15):153102.
33. Chambers I, et al. (2007) Nanog safeguards pluripotency and mediates germline development. *Nature* 450(7173):1230–1234.
34. Kalmar T, et al. (2009) Regulated fluctuations in nanog expression mediate cell fate decisions in embryonic stem cells. *PLoS Biol* 7(7):e1000149.
35. Kobayashi T, et al. (2009) The cyclic gene Hes1 contributes to diverse differentiation responses of embryonic stem cells. *Genes Dev* 23(16):1870–1875.

Supporting Information

Zhang et al. 10.1073/pnas.1305604110

SI Text

In this SI Text, we explain the derivation of Eqs. **3** and **4** in the main text and how the 3D expression for ψ_1, ψ_0 and $\xi=\cos\theta$ is obtained by extending the 2D expression of Eqs. **3** and **4** for ψ and ξ.

2D Representation of the Gene Circuit

We first derive the Langevin equations Eqs. **3** and **4** in the 2D representation of the self-regulating gene circuit. The stochastic process of gene expression in the circuit of self-regulating single gene is expressed by the master equation Eq. **1** in the main text as

$$\begin{aligned}\frac{\partial \mathbf{P}(n)}{\partial t}=&\begin{pmatrix} g_1 & 0\\ 0 & g_0\end{pmatrix}[\mathbf{P}(n-1)-\mathbf{P}(n)]\\ &+k(n+1)\mathbf{P}(n+1)-kn\mathbf{P}(n)\\ &+\begin{pmatrix} -h & f\\ h & -f\end{pmatrix}\mathbf{P}(n),\end{aligned} \quad [S1]$$

where $\mathbf{P}(n)=\begin{pmatrix}P_1(n)\\ P_0(n)\end{pmatrix}$, with $P_s(n)$ being the probability for the system having the protein copy number n at the gene state $s=0$ or 1 with the normalization $\sum_s\sum_n P_s(n)=1$. The generating function $|\Psi\rangle$ of $P_s(n)$ can be defined by using a basis set $\{|n\rangle\}$ as

$$|\Psi\rangle=\begin{pmatrix}\sum_n P_1(n)|n\rangle\\ \sum_n P_0(n)|n\rangle\end{pmatrix}. \quad [S2]$$

Then, the master equation of Eq. **1** is represented in a "second quantized" form (1–5) as

$$\frac{\partial}{\partial t}|\Psi\rangle=-\mathcal{H}|\Psi\rangle, \quad [S3]$$

where $\mathcal{H}$ is an operator having the form

$$\mathcal{H}=\begin{pmatrix} g_1 & 0\\ 0 & g_0\end{pmatrix}(1-a^\dagger)+k(a^\dagger a-a)+\begin{pmatrix} -h & f\\ h & -f\end{pmatrix}, \quad [S4]$$

with $[a,a^\dagger]=1$. We assume that the regulation factor is a dimer of product proteins, so that $h=h_0(a^\dagger)^2a^2$. We define the parameters,

$$\begin{aligned}X^{ad}&=(g_1+g_0)/(2k),\\ \delta X&=(g_1-g_0)/(2k),\\ K&=h_0/f,\\ \omega&=f/k,\end{aligned} \quad [S5]$$

where X^{ad} is the representative copy number of protein and ω is the adiabaticity parameter. By absorbing k into t (i.e., writing kt as t) in Eq. **3**, we have

$$\begin{aligned}\mathcal{H}=&\begin{pmatrix}X^{ad}+\delta X & 0\\ 0 & X^{ad}-\delta X\end{pmatrix}(1-a^\dagger)+a^\dagger a-a\\ &+\omega\begin{pmatrix}-K(a^\dagger)^2a^2 & 1\\ K(a^\dagger)^2a^2 & -1\end{pmatrix},\end{aligned} \quad [S6]$$

We consider the transition probability $P(n_f,\tau|n_i,0)$ of finding the copy number of protein n_f at time $t=\tau$ starting from n_i at $t=0$,

$$P(n_f,\tau|n_i,0)=\frac{1}{n_f!}\langle n_f|\exp\left(-\int_0^\tau dt\mathcal{H}\right)|n_i\rangle. \quad [S7]$$

$P(n_f,\tau|n_i,0)$ can be represented in a path-integral form by using an identity $1=I_s\otimes I_b$ with

$$I_b=\int_0^\infty d\psi\int_{-\pi}^{\pi}\frac{d\chi}{2\pi}|z\rangle\langle\tilde{z}|e^{-\psi}, \quad [S8]$$

where

$$|z\rangle=\exp(a^\dagger z)|0\rangle,\quad \langle\tilde{z}|=\langle 0|\exp(a\tilde{z}^*), \quad [S9]$$

with

$$z=\psi\exp(-i\chi),\quad \tilde{z}^*=\exp(i\chi),$$

and

$$I_s=\frac{1}{2\pi}\int_0^\pi\sin\theta\,d\theta\int_0^{2\pi}d\phi|\hat{s}\rangle\langle\bar{s}|, \quad [S10]$$

with

$$|\hat{s}\rangle=\begin{pmatrix}e^{i\phi/2} & \cos^2\theta/2\\ e^{-i\phi/2} & \sin^2\theta/2\end{pmatrix},\quad \langle\bar{s}|=\left(e^{-i\phi/2},e^{i\phi/2}\right). \quad [S11]$$

Note that $|z\rangle$ is the coherent state wavefunction. The corresponding $P(n)$ for $|z\rangle$ is the Poisson distribution, so that $|z|=\psi$ is the average copy number of protein of the state $|z\rangle$.

Inserting $I_s\otimes I_b$ into $P(n_f,\tau|n_i,0)$ as

$$\begin{aligned}P(n_f,\tau|n_i,0)&=\lim_{N\to\infty}\frac{1}{n_f!}\left\langle n_f\left|\prod_{r=1}^{N-1}(1-\mathcal{H}\Delta t)\right|n_i\right\rangle\\ &=\lim_{N\to\infty}\frac{1}{n_f!}\left\langle n_f|I_s\otimes I_b\prod_{r=1}^{N-1}[(1-\mathcal{H}\Delta t)I_s\otimes I_b]|n_i\right\rangle,\end{aligned} \quad [S12]$$

we have

$$P(n_f,\tau|n_i,0)=const.\int\mathcal{D}\phi\mathcal{D}\theta\mathcal{D}\psi\mathcal{D}\chi\exp\left(-\int dt\mathcal{L}\right), \quad [S13]$$

with the effective "Lagrangian,"

$$\begin{aligned}\mathcal{L}=&i\phi\frac{d}{dt}\left(\frac{1-\cos\theta}{2}\right)+i\chi\frac{d\psi}{dt}\\ &+(1-e^{i\phi})\omega\frac{1+\cos\theta}{2}K\psi^2+(1-e^{-i\phi})\omega\frac{1-\cos\theta}{2}\\ &+(1-e^{-i\chi})\psi+(1-e^{i\chi})(X^{ad}+\cos\theta\delta X).\end{aligned} \quad [S14]$$

Note that the first term, $\phi\frac{d}{dt}\left(\frac{1-\cos\theta}{2}\right)$, is the Berry phase when we consider the time-dependent closed trajectory of $\phi(t)$ and $\theta(t)$: Integration of this term represents the surface area of the sphere

of radius 1 enclosed by the closed circuit of $\phi(t)$ and $\theta(t)$, or the solid angle of that area.

Classical Approximation. The "classical" trajectory is obtained by retaining the lowest order of $\phi(t)$ and $\chi(t)$ as

$$\mathcal{L}_{cl} = i\phi\frac{\omega}{2}\left(-\frac{1}{\omega}\dot{\xi} + F(\psi,\theta)\right) + i\chi\left(\dot{\psi} + \frac{\partial U(\psi,\theta)}{\partial\psi}\right), \quad \text{[S15]}$$

where $\xi = \cos\theta$ and U is the potential,

$$U(\psi,\theta) = \frac{\psi^2}{2} - \left(X^{ad} + \xi\delta X\right)\psi, \quad \text{[S16]}$$

and F is the force

$$F(\psi,\theta) = -K(1+\xi)\psi^2 + (1-\xi). \quad \text{[S17]}$$

By putting $\mathcal{L} = \mathcal{L}_{cl}$ in Eq. **S13**, we obtain

$$P(n_f,\tau|n_i,0) = const.\int \mathcal{D}\theta\mathcal{D}\psi \prod_t \delta\left(\dot{\psi} + \frac{\partial U(\psi,\theta)}{\partial\psi}\right)\delta\left(-\frac{1}{\omega}\dot{\xi} + F(\psi,\theta)\right), \quad \text{[S18]}$$

which leads to the deterministic equations,

$$\dot{\psi} = -\frac{\partial U(\psi,\theta)}{\partial\psi}, \quad \text{[S19]}$$

$$\frac{1}{\omega}\dot{\xi} = F(\psi,\theta). \quad \text{[S20]}$$

The classical trajectory is the sequence of the continuously changing (or stationary) Poisson distributions. In the adiabatic limit of $\omega\to\infty$, the DNA state θ is determined by the equilibrium relation, $F(\psi,\theta) = 0$.

Semiclassical Approximation. In the next level of approximation (i.e., in the "semiclassical" approximation), the Lagrangian is obtained by retaining the second-order terms of $\chi(t)$ and $\phi(t)$ as

$$\mathcal{L} = \mathcal{L}_{cl} - \frac{1}{2}(i\chi)^2\left(\psi + X^{ad} + \xi\delta X\right) - \frac{\omega}{4}(i\phi)^2\left(K(1+\xi)\psi^2 + (1-\xi)\right). \quad \text{[S21]}$$

Using the Hubbard–Stratonovich transformation (6),

$$\exp\left((i\chi)^2 J_1 dt\right) = \frac{1}{\sqrt{2\pi}}\int_{-\infty}^{\infty} dy_1 \exp\left(-\frac{y_1^2}{2} + \sqrt{2J_1 dt}\,(i\chi)y_1\right),$$

and

$$\exp\left((i\phi)^2 J_2 dt\right) = \frac{1}{\sqrt{2\pi}}\int dy_2 \exp\left(-\frac{y_2^2}{2} + \sqrt{2J_2 dt}\,(i\phi)y_2\right), \quad \text{[S22]}$$

with

$$J_1 = \frac{1}{2}\left(\psi + X^{ad} + \xi\delta X\right), \qquad J_2 = \frac{\omega}{4}\left(K(1+\xi)\psi^2 + (1-\xi)\right), \quad \text{[S23]}$$

we have

$$P(n_f,\tau|n_i,0) = const.\int \mathcal{D}\theta\mathcal{D}\psi\mathcal{D}y_1\mathcal{D}y_2 \exp\left(-\int dt\,\frac{y_1^2+y_2^2}{2}\right)\prod_t \delta\left(\dot{\psi} + \frac{\partial U(\psi,\theta)}{\partial\psi} + \sqrt{2J_1/dt}\,y_1\right) \times \delta\left(-\frac{1}{\omega}\dot{\xi} + F(\psi,\theta) + \frac{2\sqrt{2J_2/dt}}{\omega}y_2\right), \quad \text{[S24]}$$

which leads to the coupled-Langevin equations,

$$\dot{\psi} = -\psi + X^{ad} + \xi\delta X + \eta_\psi, \quad \text{[S25]}$$

$$\frac{1}{\omega}\dot{\xi} = -K(1+\xi)\psi^2 + (1-\xi) + \eta_\theta, \quad \text{[S26]}$$

where η_ψ and η_θ are Gaussian random numbers with $<\eta_\psi> = 0$, $\langle\eta_\theta\rangle = 0$, and

$$\langle\eta_\psi(t)\eta_\psi(t')\rangle = \left(\psi + X^{ad} + \xi\delta X\right)\delta(t-t'), \qquad \langle\eta_\theta(t)\eta_\theta(t')\rangle = \frac{2}{\omega}\left(K(1+\xi)\psi^2 + (1-\xi)\right)\delta(t-t'). \quad \text{[S27]}$$

In the strong adiabatic limit, we can see that Eq. **S26** returns to $F(\psi,\theta) = 0$ as expected. η_θ in Eq. **S26** represents the "eddy" or "churn" effect of nonadiabaticity. If we rewrite Eq. **S25** by using the system volume Ω_0 and defining $\rho = \psi/\Omega_0$, $x^{ad} = X^{ad}/\Omega_0$, $\delta x = \delta X/\Omega_0$, and $\kappa = K\Omega_0^2$, the Langevin equations are more symmetrical as

$$\dot{\rho} = -\rho + x^{ad} + \xi\delta x + \epsilon_\rho, \quad \text{[S28]}$$

$$\frac{1}{\omega}\dot{\xi} = -\kappa(1+\xi)\rho^2 + (1-\xi) + \epsilon_\theta, \quad \text{[S29]}$$

and

$$\langle\epsilon_\rho(t)\epsilon_\rho(t')\rangle = \frac{1}{\Omega_0}\left(\rho + x^{ad} + \xi\delta x\right)\delta(t-t'), \qquad \langle\epsilon_\theta(t)\epsilon_\theta(t')\rangle = \frac{2}{\omega}\left(\kappa(1+\xi)\rho^2 + (1-\xi)\right)\delta(t-t'), \quad \text{[S30]}$$

which are Eqs. **3** and **4** in the main text. By solving these equations, we can obtain the various types of time correlation functions and the 2D distribution, $P_\theta(\psi)$, discussed in the main text.

Extension to the 3D Representation

We start from Eq. **S7** but in this time we consider the identity

$$1 = I_{b1} = \int_0^\infty d\psi_1 \int_{-\pi}^{\pi}\frac{d\chi_1}{2\pi}|z_1\rangle\langle\widetilde{z_1}|, \quad \text{[S31]}$$

for the case that the regulatory protein is not bound to DNA, and

$$1 = I_{b0} = \int_0^\infty d\psi_0 \int_{-\pi}^{\pi}\frac{d\chi_0}{2\pi}|z_0\rangle\langle\widetilde{z_0}|, \quad \text{[S32]}$$

for the case that the regulatory protein is bound to DNA, where

$$|z_1\rangle = \exp\left(a^\dagger z_1 - z_1 \tilde{z_1}^*\right)|0\rangle, \quad \langle \tilde{z_1}| = \langle 0|\exp\left(a\tilde{z_1}^*\right), \qquad \text{[S33]}$$

and

$$|z_0\rangle = \exp\left(a^\dagger z_0 - z_0 \tilde{z_0}^*\right)|0\rangle, \quad \langle \tilde{z_0}| = \langle 0|\exp\left(a\tilde{z_0}^*\right), \qquad \text{[S34]}$$

with $z_1 = \psi_1 \exp(-i\chi_1)$, $\tilde{z_1}^* = \exp(i\chi_1)$, $z_0 = \psi_0 \exp(-i\chi_0)$, and $\tilde{z_0}^* = \exp(i\chi_0)$. Then, instead of using $I_s \otimes I_b$ of the previous section, we use a form of

$$1 = I_{sb} = \int_0^\infty d\psi_0 d\psi_1 \int_{-\pi}^{\pi} \frac{d\chi_0 d\chi_1}{2\pi}\frac{1}{2\pi}\int_0^\pi \sin\theta d\theta \int_0^{2\pi} d\phi \begin{pmatrix} e^{i\phi/2}\cos^2\theta/2|z_1\rangle \\ e^{-i\phi/2}\sin^2\theta/2|z_0\rangle \end{pmatrix}\left(\langle\tilde{z_1}|e^{-i\phi/2}, \langle\tilde{z_0}|e^{i\phi/2}\right). \qquad \text{[S35]}$$

Here, $\psi_1 = \langle\tilde{z_1}|a^\dagger a|z_1\rangle$ and $\psi_0 = \langle\tilde{z_0}|a^\dagger a|z_0\rangle$. ψ_1 and ψ_0 are, therefore, the expectation values of the copy number of proteins in the DNA unbound and bound states, respectively, when the Poisson distributions for the number of proteins are assumed (the coherent state represents the Poisson distribution). The classical trajectory is the sequence of the continuously changing (or stationary) Poisson distributions.

Inserting I_{sb} of Eq. **S35** into $P(n_{1f}, n_{0f}, \tau|n_{1i}, n_{0i}, 0)$, we have

$$\begin{aligned} &P(n_{1f}, n_{0f}, \tau|n_{1i}, n_{0i}, 0) \\ &= \lim_{N\to\infty}\left(\frac{\langle n_{1f}|}{n_{1f}!}, \frac{\langle n_{0f}|}{n_{0f}!}\right)\prod_{r=1}^{N-1}(1-\mathcal{H}\Delta t)\begin{pmatrix}|n_{1i}\rangle \\ |n_{0i}\rangle\end{pmatrix} \\ &= \lim_{N\to\infty}\left(\frac{\langle n_{1f}|}{n_{1f}!}, \frac{\langle n_{0f}|}{n_{0f}!}\right) I_{sb}\prod_{r=1}^{N-1}[(1-\mathcal{H}\Delta t)I_{sb}]\begin{pmatrix}|n_{1i}\rangle \\ |n_{0i}\rangle\end{pmatrix}. \end{aligned} \qquad \text{[S36]}$$

Then, $P(n_{1f}, n_{0f}, \tau|n_{1i}, n_{0i}, 0)$ is represented by the path-integral form,

$$P(n_f, \tau|n_i, 0) = const \int \mathcal{D}\phi\mathcal{D}\theta\mathcal{D}\psi_1\mathcal{D}\psi_0\mathcal{D}\chi_1\mathcal{D}\chi_0 \exp\left(-\int d t\mathcal{L}\right), \qquad \text{[S37]}$$

with the effective Lagrangian,

$$\begin{aligned} \mathcal{L} = {} & i\phi\frac{d}{dt}\left(\sin^2\frac{\theta}{2}\right) \\ & + i\chi_1\frac{d}{dt}\left(\psi_1\cos^2\frac{\theta}{2}\right) + i\chi_0\frac{d}{dt}\left(\psi_0\sin^2\frac{\theta}{2}\right) \\ & + \omega K\psi_1^2(1-\exp[F_1+i\phi])\cos^2\frac{\theta}{2} \\ & + \omega(1-\exp[F_0-i\phi])\sin^2\frac{\theta}{2} \\ & + \left(1-e^{-i\chi_1}\right)\psi_1\cos^2\frac{\theta}{2} + \left(1-e^{-i\chi_0}\right)\psi_0\sin^2\frac{\theta}{2} \\ & + \left(1-e^{i\chi_1}\right)\left(X^{ad}+\delta X\right)\cos^2\frac{\theta}{2} \\ & + \left(1-e^{i\chi_0}\right)\left(X^{ad}-\delta X\right)\sin^2\frac{\theta}{2}, \end{aligned} \qquad \text{[S38]}$$

where $F_1 = 2i(\chi_0-\chi_1) + \psi_1(e^{i(\chi_0-\chi_1)}-1)$ and $F_0 = \psi_0(e^{i(\chi_1-\chi_0)}-1)$. Note that this expression is reduced to the Lagrangian Eq. **S14** when we put $\psi_1 = \psi_0$ and $\chi_1 = \chi_0$.

Classical Approximation. The classical trajectory is obtained by retaining the lowest order of $\phi(t)$, $\chi_1(t)$, and $\chi_0(t)$ as

$$\begin{aligned} \mathcal{L}_{cl} = {} & i\phi\left[\frac{d}{dt}\left(\sin^2\frac{\theta}{2}\right) - \omega\left(K\psi_1^2\cos^2\frac{\theta}{2} - \sin^2\frac{\theta}{2}\right)\right] \\ & + i\chi_1\left[\frac{d}{dt}\left(\psi_1\cos^2\frac{\theta}{2}\right) - \left(X^{ad}+\delta X-\psi_1\right)\cos^2\frac{\theta}{2}\right. \\ & \left. + \omega\left(K\psi_1^2 G_1\cos^2\frac{\theta}{2} - \psi_0\sin^2\frac{\theta}{2}\right)\right] \\ & + i\chi_0\left[\frac{d}{dt}\left(\psi_0\sin^2\frac{\theta}{2}\right) - \left(X^{ad}-\delta X-\psi_0\right)\sin^2\frac{\theta}{2}\right. \\ & \left. - \omega\left(K\psi_1^2 G_1\cos^2\frac{\theta}{2} - \psi_0\sin^2\frac{\theta}{2}\right)\right], \end{aligned} \qquad \text{[S39]}$$

where $G_1 = (\psi_1+2)$. By writing $\xi = \cos\theta$, $\overline{\psi} = (\psi_1+\psi_0)/2$, $\hat{\psi} = (\psi_1-\psi_0)/2$, $\psi = \psi_1\cos^2\frac{\theta}{2} + \psi_0\sin^2\frac{\theta}{2} = \overline{\psi} + \xi\hat{\psi}$, $\overline{\chi} = (\chi_1+\chi_0)/2$, and $\hat{\chi} = (\chi_1-\chi_0)/2$, the classical Lagrangian is

$$\begin{aligned} \mathcal{L}_{cl} = {} & i\phi\left[\frac{d}{dt}\left(\sin^2\frac{\theta}{2}\right) - \omega\left(K\psi_1^2\cos^2\frac{\theta}{2} - \sin^2\frac{\theta}{2}\right)\right] \\ & + i\overline{\chi}\left[\frac{d}{dt}\psi - \left(X^{ad}+\xi\delta X-\psi\right)\right], \\ & + i\hat{\chi}\left[\frac{d}{dt}\left(\xi\overline{\psi}+\hat{\psi}\right) - \left(\xi X^{ad}+\delta X-\xi\overline{\psi}-\hat{\psi}\right)\right. \\ & \left. + \omega\left\{K\psi_1^2(\psi_1+2)(1+\xi) - \psi_0(1-\xi)\right\}\right]. \end{aligned} \qquad \text{[S40]}$$

Then, the classical equations are obtained as

$$\frac{d}{dt}\psi = X^{ad} + \xi\delta X - \psi, \qquad \text{[S41]}$$

$$\begin{aligned} \frac{1}{\omega}\frac{d}{dt}\left(\xi\overline{\psi}+\hat{\psi}\right) = {} & \frac{1}{\omega}\left[\left(\xi X^{ad}+\delta X\right) - \left(\xi\overline{\psi}+\hat{\psi}\right)\right] \\ & - K\psi_1^2(1+\xi)(\psi_1+2) + (1-\xi)\psi_0, \end{aligned} \qquad \text{[S42]}$$

$$\frac{1}{\omega}\frac{d}{dt}\xi = -K\psi_1^2(1+\xi) + (1-\xi). \qquad \text{[S43]}$$

Note that Eq. **S41** is the same as Eq. **S19**, and Eq. **S43** is obtained by replacing ψ in Eq. **S20** with $\psi_1 = \overline{\psi} + \hat{\psi}$. Eq. **S42** is a new one, representing the nonadiabatic effects.

We can see that Eqs. **S41**–**S43** behave suitably in both the adiabatic and nonadiabatic limits: In the adiabatic limit of large ω, terms of $1/\omega$ become small and we have,

$$\frac{d}{dt}\psi = \left(X^{ad}+\xi\delta X\right) - \psi, \qquad \text{[S44]}$$

$$0 = -K\psi_1^2(1+\xi)(\psi_1+2) + (1-\xi)\psi_0, \qquad \text{[S45]}$$

$$0 = -K\psi_1^2(1+\xi) + (1-\xi). \qquad \text{[S46]}$$

By inserting Eq. **S46** into Eq. **S45**, we find $\psi_1 + 2 = \psi_0$. This result is reasonable when we consider that in the state 1 all

copies of the regulatory protein are in the solution, but in the state 0 a dimer protein is absorbed onto DNA and is lost from the solution. In this adiabatic limit, therefore, we essentially have $\psi_1 \approx \psi_0$.

In the nonadiabatic limit of small ω, however, $1/\omega$ terms dominate, so that

$$\frac{d}{dt}\psi = (X^{ad} + \xi\delta X) - \psi, \qquad \text{[S47]}$$

$$\frac{d}{dt}\left(\xi\overline{\psi} + \hat{\psi}\right) = \left[\left(\xi X^{ad} + \delta X\right) - \left(\xi\overline{\psi} + \hat{\psi}\right)\right], \qquad \text{[S48]}$$

$$\frac{d}{dt}\xi = 0. \qquad \text{[S49]}$$

From Eq. **S49**, $\theta = const.$ and we can see $\overline{\psi} = X^{ad}$ and $\hat{\psi} = \delta X$, that is, $\psi_1 = X^{ad} + \delta X$ and $\psi_0 = X^{ad} - \delta X$ satisfy Eqs. **S47** and **S48**, which are the expected results for the nonadiabatic limit.

Semiclassical Approximation. In the next level of approximation (i.e., in the semiclassical approximation), the Lagrangian is obtained by retaining the second-order terms of $\phi(t)$, $\chi_1(t)$, and $\chi_0(t)$ as $\mathcal{L} = \mathcal{L}_{cl} + \mathcal{L}_G$ with

$$\begin{aligned}\mathcal{L}_G = &-\frac{\omega}{4}(i\phi)^2\left(K(1+\xi)\psi_1^2 + (1-\xi)\right)\\ &-\frac{1}{2}[i(\chi_0 - \chi_1)](i\phi)\omega\left(K(1+\xi)\psi_1^2(\psi_1+2) + (1-\xi)\psi_0\right)\\ &-\frac{1}{4}(i\chi_1)^2(1+\xi)\left(\psi_1 + X^{ad} + \delta X\right)\\ &-\frac{1}{4}(i\chi_0)^2(1-\xi)\left(\psi_0 + X^{ad} - \delta X\right)\\ &-\frac{1}{4}[i(\chi_0 - \chi_1)]^2\omega\left(K(1+\xi)\psi_1^2 f + (1-\xi)g\right),\end{aligned} \qquad \text{[S50]}$$

where $f = \psi_1^2 + 5\psi_1 + 4$ and $g = \psi_0^2 + \psi_0$.

Using $\overline{\chi} = (\chi_1 + \chi_0)/2$ and $\hat{\chi} = (\chi_1 - \chi_0)/2$, Eq. **S50** can be rewritten as

$$\begin{aligned}\mathcal{L}_G = &-\frac{\omega}{4}(i\phi)^2\left(K(1+\xi)\psi_1^2 + (1-\xi)\right)\\ &+ (i\hat{\chi})(i\phi)\omega\left(K(1+\xi)\psi_1^2(\psi_1+2) + (1-\xi)\psi_0\right)\\ &-(i\hat{\chi})^2\omega\left(K(1+\xi)\psi_1^2 f + (1-\xi)g\right)\\ &-\frac{1}{2}\left[(i\overline{\chi})^2 + (i\hat{\chi})^2\right](\psi + X^{ad} + \xi\delta X)\\ &-(i\overline{\chi})(i\hat{\chi})\left(\hat{\psi} + \delta X + \xi(\overline{\psi} + X^{ad})\right).\end{aligned} \qquad \text{[S51]}$$

By defining a vector,

$$i\varphi = \begin{pmatrix} i\phi \\ i\hat{\chi} \\ i\overline{\chi} \end{pmatrix}, \qquad \text{[S52]}$$

Eq. **S51** is written as $\mathcal{L}_G = -\frac{1}{2}(i\varphi^\dagger)Q(i\varphi)$ with

$$Q = \begin{pmatrix} \frac{\omega}{2}(A+B) & -\omega(A(\psi_1+2) + B\psi_0) & 0 \\ -\omega(A(\psi_1+2) + B\psi_0), & 2\omega(Af + Bg) + \left(\psi + X^{ad} + \xi\delta X\right), & \hat{\psi} + \delta X + \xi\left(\overline{\psi} + X^{ad}\right) \\ 0 & \hat{\psi} + \delta X + \xi\left(\overline{\psi} + X^{ad}\right) & \psi + X^{ad} + \xi\delta X \end{pmatrix}, \qquad \text{[S53]}$$

where $A = K(1+\xi)\psi_1^2$ and $B = 1 - \xi$. The Hubbard–Stratonovich transformation we should consider is based on the Gaussian integral for the vector $y^\dagger = (y_p, y_h, y_b)$ as

$$\int_{-\infty}^{\infty} dy\, \exp\left(-\frac{1}{2}(y - i\varphi)^\dagger Q(y - i\varphi)dt\right) = \frac{(2\pi/dt)^{\frac{3}{2}}}{(\det Q)^{\frac{1}{2}}}. \qquad \text{[S54]}$$

Because $Q^\dagger = Q$, we have

$$\exp\left(\frac{1}{2}(i\varphi^\dagger)Q(i\varphi)dt\right) = \frac{(\det Q)^{\frac{1}{2}}}{(2\pi/dt)^{\frac{3}{2}}}\int_{-\infty}^{\infty} dy\, \exp\left(-\frac{1}{2}y^\dagger Q y dt + (i\varphi)^\dagger Q y dt\right). \qquad \text{[S55]}$$

This expression leads to the coupled-Langevin equations,

$$\dot{\psi} = -\psi + X^{ad} + \xi\delta X + \eta_3, \qquad \text{[S56]}$$

$$\begin{aligned}\frac{d}{dt}\left(\xi\overline{\psi} + \hat{\psi}\right) = &\xi X^{ad} + \delta X - \left(\xi\overline{\psi} + \hat{\psi}\right)\\ &-\omega\left[K\psi_1^2(\psi_1+2)(1+\xi) - \psi_0(1-\xi)\right] + \eta_2,\end{aligned} \qquad \text{[S57]}$$

$$\frac{1}{\omega}\dot{\xi} = -K(1+\xi)\psi_1^2 + (1-\xi) + \eta_1. \qquad \text{[S58]}$$

Here, η_1, η_2, and η_3 are

$$\begin{aligned}\eta_1 &= \frac{2}{\omega}\left(Q_{11}y_p + Q_{21}y_h\right),\\ \eta_2 &= Q_{21}y_p + Q_{22}y_h + Q_{23}y_b,\\ \eta_3 &= Q_{32}y_h + Q_{33}y_b,\end{aligned} \qquad \text{[S59]}$$

with Q_{ij} being the (i,j)component of the matrix Q. y_b, y_h, and y_p are Gaussian random numbers with $\langle y_b\rangle = \langle y_h\rangle = \langle y_p\rangle = 0$, and

$$\begin{aligned}&\langle y_p(t)y_p(t')\rangle = \frac{\delta_{tt'}}{dt}(Q^{-1})_{11}, \quad \langle y_h(t)y_h(t')\rangle = \frac{\delta_{tt'}}{dt}(Q^{-1})_{22}\\ &\langle y_b(t)y_b(t')\rangle\frac{\delta_{tt'}}{dt}(Q^{-1})_{33}, \quad \langle y_p(t)y_h(t')\rangle = \frac{\delta_{tt'}}{dt}(Q^{-1})_{12},\\ &\langle y_p(t)y_b(t')\rangle = \frac{\delta_{tt'}}{dt}(Q^{-1})_{13}, \quad \langle y_h(t)y_b(t')\rangle = \frac{\delta_{tt'}}{dt}(Q^{-1})_{23}.\end{aligned} \qquad \text{[S60]}$$

In the limit of $dt \to 0$, $\frac{\delta_{tt'}}{dt}$ in the above expression will approach $\delta(t-t')$. If we want to go back to the expression of ψ_1 and ψ_0, we can use

$$\psi = \psi_1 \cos^2\frac{\theta}{2} + \psi_0 \sin^2\frac{\theta}{2},$$
$$\xi\overline{\psi} + \hat{\psi} = \psi_1 \cos^2\frac{\theta}{2} - \psi_0 \sin^2\frac{\theta}{2}, \qquad \textbf{[S61]}$$
$$\xi = \cos\theta.$$

In this way, Eqs. **S56**–**S60** are the extension of Eqs. **S28**–**S30**. By solving Eqs. **S56**–**S60**, we can obtain the distribution $P_\theta(\psi_1, \psi_0)$. Eqs. **S56**–**S60** give quantitatively better results than Eqs. **S28**–**S30**, although the qualitative features of the results obtained with Eqs. **S56**–**S60** are the same as those obtained with Eqs. **S28**–**S30**.

1. Mattis DC, Glasser ML (1998) The uses of quantum field theory in diffusion-limited reactions. *Rev Mod Phys* 70(3):979–1001.
2. Doi M (1976) Second quantization representation for classical many-particle system. *J Phys Math Gen* 9(9):1465–1477.
3. Doi M (1976) Stochastic theory of diffusion-controlled reaction. *J Phys Math Gen* 9(9):1479–1495.
4. Peliti L (1985) Path integral approach to birth-death processes on a lattice. *J Phys* 46(9):1469–1483.
5. Sasai M, Wolynes PG (2003) Stochastic gene expression as a many-body problem. *Proc Natl Acad Sci USA* 100(5):2374–2379.
6. Itakura K, Ohkubo J, Sasa S-I (2010) Two Langevin equations in the Doi-Peliti formalism. *J Phys A Math Theor* 43(12):125001.

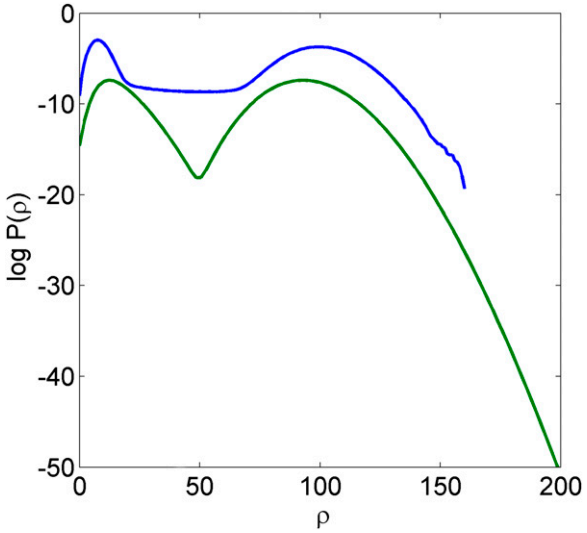

Fig. S1. Distribution of protein density ρ for $\omega = 0.001$ calculated from the Langevin dynamics in the extended dimensional space (Eqs. **3** and **4** in the main text, green line) is compared with the one calculated with the Gillespie algorithm from the master equation (Eq. **1** in the main text, blue line).

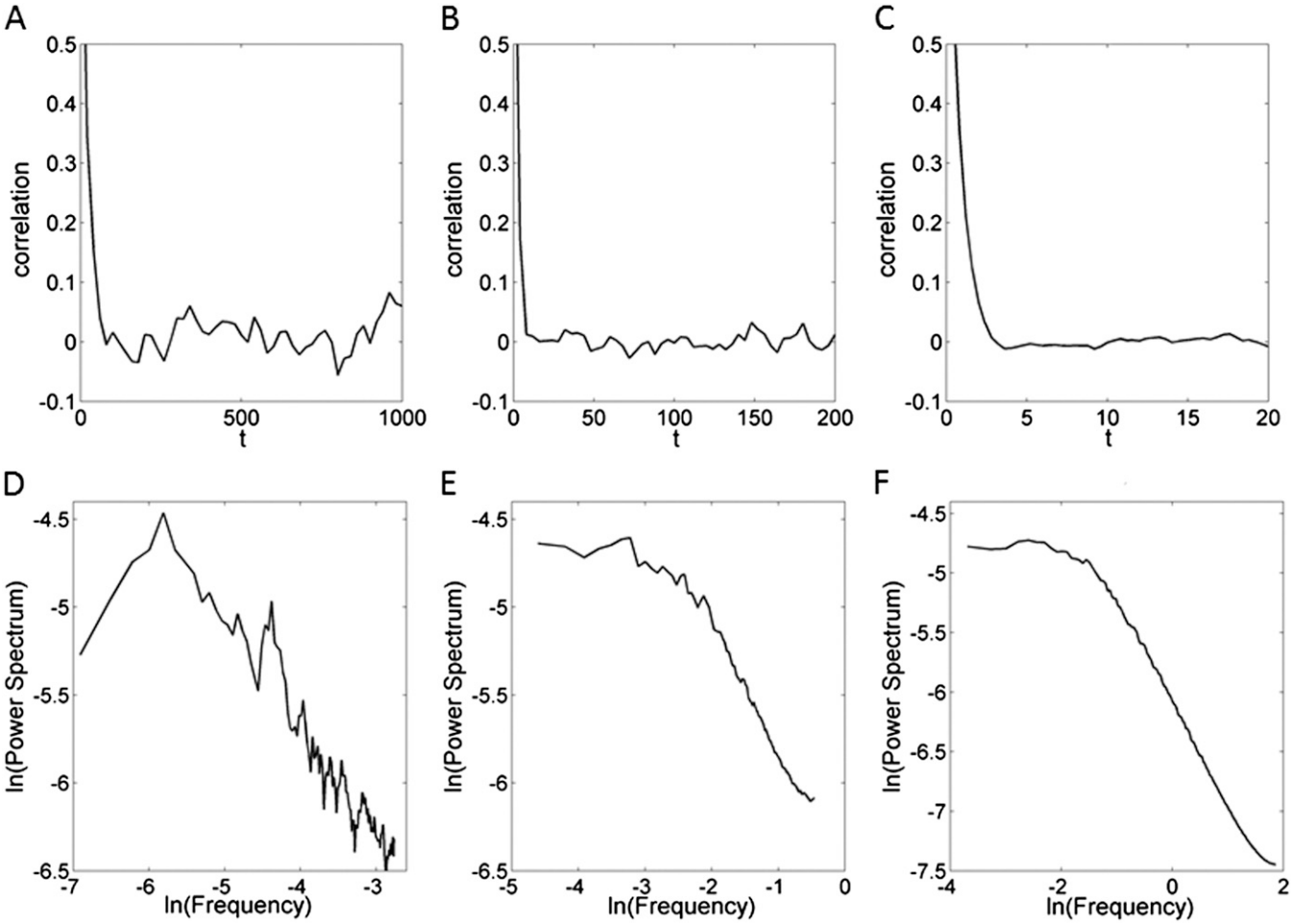

Fig. S2. The two time correlation functions in protein concentration and their Fourier transformation. The correlation functions (*A*–*C*) and their Fourier spectra (*D*–*F*) are calculated with Eqs. **3** and **4** in the main text with (*A* and *D*) $\omega = 0.01$, (*B* and *E*) $\omega = 0.1$, and (*C* and *F*) $\omega = 100$. The Fourier spectra are shown in the log-log plot.